Carbon 230 (2024) 119555

Contents lists available at ScienceDirect

Carbon

journal homepage: www.elsevier.com/locate/carbon

Research paper

Tuning the adhesion of diamond/copper interfaces through surface chemical modifications and reconstruction

Elisa Damiani, Margherita Marsili, M. Clelia Righi *

Department of Physics and Astronomy, University of Bologna, Viale Carlo Berti Pichat 6/2, Bologna, 40127, Italy

ARTICLE INFO

Keywords:
Adhesion
DLCs
Diamond-copper interfaces
Density functional theory
Chemical modifications

ABSTRACT

Diamond and diamond-like carbon (DLC) coatings are well-known for their exceptional combination of tribological and mechanical properties, such as low friction coefficients and wear rates, together with high hardness and elastic modulus. A significant limitation in their employment concerns their spallation from the substrate; it is thus interesting to explore how DLCs adhesion can be tuned through chemical modifications of its surfaces. We employ *ab initio* simulations to study the effect of surface reconstruction and chemical species intercalation (B, P, O, F, N, S, H) on the adhesion of non-reconstructed and Pandey-reconstructed C(111)/Cu(111) interfaces. We found that the increment of graphitization at the diamond surface decreases the adhesion. Moreover, when a high degree of surface graphitization is present the best way to increase adhesion is to select atoms able to act as chemical bridges (e.g., B and N), compensating for the lack of interaction between the surfaces. Conversely, adhesion reduction of ~100% can be achieved, regardless of the degree of surface graphitization, by intercalating an atomic species that does not bond with the countersurface and prevents the interaction between the slabs, i.e. F and S.

1. Introduction

Diamond and diamond-like carbon (DLC) coatings represent an important class of solid lubricants that, exploiting the outstanding properties of diamond [1–3], provide some of the lowest known friction coefficients and wear rates [4], typically in the range of 0.01–0.5 and of 10^{-7}-10^{-9} mm^3/N·m, respectively [5]. For these reasons, they are largely used in industry to reduce friction and wear in engine components, to avoid stiction in micro- and nano-electromechanical systems (MEMS and NEMS) and to increase the longevity and functionality of biological implants and industrial cutting tools [6,7].

Often the main limitation on the development of carbon coating technologies is due to poor adhesion between the diamond film and the material which would otherwise benefit from the presence of the coating for better structural, thermal, or opto-electronic performances [8]. Indeed, poor adhesion can easily result in spallation of the film from the substrate, making the coating useless [9–11]. On the other hand, to reduce friction, quenching the adhesion with any countersurface would be highly desirable [12]. Tailoring the substrate/coating or coating/countersurface adhesion is therefore needed to fully exploit the potentiality of this unique material. A possible way to tune the adhesion between two materials is to chemically modify their surfaces. Indeed, everyday, lubricant additives play exactly this role in our car engines: by dissociating in tribological conditions and chemically binding to the surfaces of the mechanical components these molecules reduce micro-asperity adhesion and avoid our engines from gripping [13].

In this work, diamond/copper interfaces adhesion is studied, considering also the impact of surface modifications due to reconstruction and adatom adsorption. The aim is not to simulate a system as close to reality as possible, but to understand basic mechanisms that should qualitatively apply in other situations as well. Copper was chosen as a representative of transition metals, which have a partially filled d-shell. Although each metal has its own specific electronic properties we expect our results to be rather general for the broad class of diamond/transition metal interfaces, as it was shown in Ref. [14] for homogeneous metal–metal interfaces. Indeed, it was found that the overall effect of adatoms on adhesion, i.e. whether they enhanced or reduced it, was independent of the chosen metal [14]. In particular, the study takes into account the interfaces between Cu(111), the most stable surface of copper (surface energy γ of 1.31 J/m^2), and two relevant (111) diamond surfaces able to represent the type of dangling bonds and the electronic configuration of other low-index diamond faces, such as (110) and (100) [15,16]: the non-reconstructed (1 × 1) surface with dangling bond (DB) termination (γ=5.04 J/m^2), which has a sp^3 bond structure, and the Pandey-reconstructed (2 × 1) (γ=3.47 J/m^2), which, with its delocalized π electrons, is representative of the

* Corresponding author.
E-mail address: clelia.righi@unibo.it (M.C. Righi).

https://doi.org/10.1016/j.carbon.2024.119555
Received 3 May 2024; Received in revised form 1 August 2024; Accepted 19 August 2024
Available online 22 August 2024
0008-6223/© 2024 The Authors. Published by Elsevier Ltd. This is an open access article under the CC BY license (http://creativecommons.org/licenses/by/4.0/).

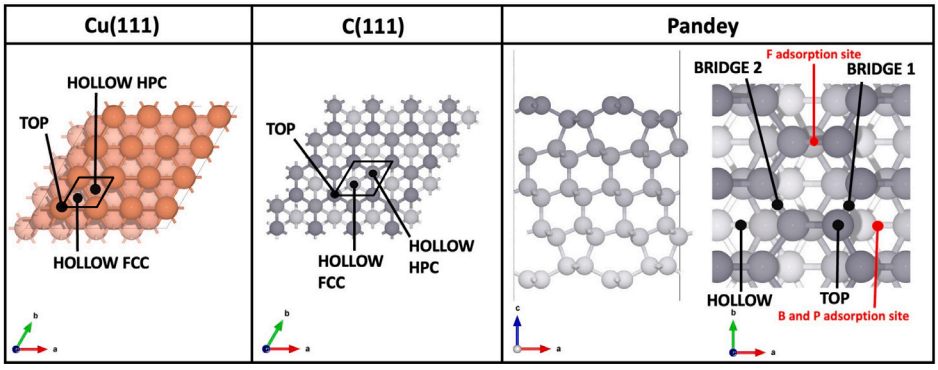

Fig. 1. Top views of Cu(111), C(111) and Pandey surfaces. For the Pandey, also the lateral view is shown. In all cases, surface atoms are the darker ones. The high symmetry points are indicated in black: while, the peculiar adsorption sites of fluorine, boron and phosphorus on Pandey are highlighted in red. (For interpretation of the references to color in this figure legend, the reader is referred to the web version of this article.)

sp^2 aromatic or graphitic layer often detected on the diamond/DLC surface during rubbing. It is known, indeed, that the sp^3/sp^2 bond ratio is a fundamental parameter that influences the properties of amorphous carbon films, such as hardness, strength and adhesion [5,17].

Chemical modifications of the surfaces are introduced through the intercalation of atomic species between the two slabs as simple adatoms. Although stable, this may not be the most energetically favorable geometry (with respect to substitutional or interstitial sites). For all the cases, however, our primary focus here is to identify the basic mechanisms at play when the adhesion between the two surfaces is enhanced or quenched, keeping the systems as simple as possible. B, P, O, F, H, N, S have been chosen as chemical species following different criteria: O and H are common contaminants, F, S, and P are well known elements within the tribological community as they are present with a prominent role in lubricants additives, B and N have been chosen for their use as dopants. We considered a 25% of coverage, since it is the most favorable configuration for adsorption on metals [14,18–20] and, typically, the effect of the atom on the adhesion energy variation is amplified with the coverage [14]. Thus, we expect that our general trends, i.e. whether a chemical species reduces or improves C/Cu adhesion, can be extended also to 50% and 100% coverages.

The paper is organized as follows: after a brief introduction on the methodology and on the computational details, results are presented and discussed. In particular, starting from the Bond Order analysis of the clean surfaces and characterizing their reactivity, the adatom adsorption process is analyzed. Then the effect of surface reconstruction and adatom adsorption on the interface adhesion is studied and interpreted in terms of Bond Order analysis. Conclusions are finally drawn.

2. Methods

First-principles calculations are performed using the Vienna Ab initio Simulation Package (VASP) [21–23], employing PBE-GGA exchange–correlation functionals [24]. All calculations are spin-polarized with a plane wave cutoff energy of 400 eV (a kinetic energy cutoff providing total energies and lattice parameters converged by 0.02 eV/atom and 0.02%, respectively). A 0.03 eV Gaussian smearing is employed.

The adatoms are adsorbed on 2 × 2 slabs in order to study a 25% of coverage. The C(111) and Cu(111) surfaces are modeled by slabs with 10 and 6 atomic planes, respectively, ensuring converged values of the surface energies. A vacuum region of about 15 Å is included in the supercell.

For adsorption calculations, converged Γ-centered grids of 10 × 10 × 1 and of 13 × 13 × 1 are used for systems with C(111) and Cu(111) surfaces, respectively. During relaxation, only the central atomic layer of the slab is fixed, while all the other atoms are allowed to move in all directions (a schematic representation is shown in Fig. 1 of the S.I.). Energies and atomic forces are converged within 10^{-6} eV and 0.05 eV/Å, respectively.

When simulating the interfaces, to identify a common supercell accommodating both lattices while keeping the mismatch below a given threshold value and the supercell size as low as possible, we employed the Zur algorithm [25] and distributed the residual strain between the two faces in such a way that it is inversely proportional to their bulk modulus (bulk modulus values of 436 GPa and 139 GPa for C and Cu, respectively). We tested the effect of this procedure on the energetics of our systems, comparing it with a scenario where all the strain is applied exclusively to copper (see Section 2 of S.I. for the analysis). In the case of Cu(111) and C(111) the lattice parameters are very close, namely 2.57 Å and 2.52 Å respectively; indeed the Zur algorithm provides a 1 × 1 supercell without any relative rotation between the two lattices. This procedure leads to an effective deformation of the diamond slab of 0.65%, which results in a residual internal stress of 1.9 GPa, compatible to experimental values for DLC coatings [26–30].

All interfaces are optimized through full relaxation calculations, employing a 14 × 14 × 1 Γ-centered grid (combining the results on the convergence tests of the slabs and optimal computational load distribution). 2 × 2 supercells with hexagonal and orthorhombic geometries are employed for non-reconstructed and Pandey-reconstructed diamond/copper interfaces, respectively. The screening for the optimal relative lateral displacement is performed with looser convergence parameters (10^{-4} eV for the energies and 0.1 eV/Å for atomic forces) and only the configuration with the lowest total energy is further relaxed with more accurate convergence parameters (10^{-6} eV for the energies and 0.05 eV/Å for atomic forces).

For each interface, we calculated the bond orders between couple of atoms using the DDEC6 atomic population analysis method, that is a refinement of the Density Derived Electrostatic and Chemical (DDEC) approach, implemented in the CHARGEMOL program [31]. The DDEC method is an atoms-in-materials (AIM) partitioning scheme, where the total electronic density $n(\mathbf{r})$ is divided into overlapping atomic densities $n_i(\mathbf{r})$ that can be defined in terms of a weighting factor, $w_i(\mathbf{r}) \geq 0$, such that:

$$n_i(\mathbf{r}) = \frac{w_i(\mathbf{r})}{\sum_k w_k(\mathbf{r})} n(\mathbf{r}) \quad (1)$$

where the sum runs over all atoms in the cell plus their periodic images along any direction. Once the electron density distribution of atom i ($n_i(\mathbf{r})$) in a material has been found, its net atomic charge Q_i can be obtained by integrating $n_i(\mathbf{r})$ over all space:

$$Q_i = z_i - N_i = z_i - \int n_i(r) d^3 r \quad (2)$$

where N_i is the number of electrons assigned to atom i and z_i is its effective nuclear charge [32]. In the DDEC method, the weighting

Table 1
Sum of bond orders (SBO) per atom ranging from the surface to the central layer of Cu(111), C(111) and Pandey. Since the Pandey geometry displays different SBO values for atoms in the same layer, we calculated the average and semidispersion.

Cu(111)	SBO	C(111)	SBO	Pandey	SBO (avg.)	Semidispersion
layer 1 (surf)	2.7	layer 1 (surf)	3.4	layer 1 (surf)	3.8	0
layer 2	3.1	layer 2	3.9	layer 2	3.6	0.02
layer 3 (bulk)	3.1	layer 3	3.6	layer 3	3.6	0.04
		layer 4	3.7	layer 4	3.7	0.11
		layer 5 (bulk)	3.7	layer 5 (bulk)	3.7	0.09

function is designed so that the atomic weights are optimized to mimic both the spherical average of $n_i(\mathbf{r})$ and the density of a reference ion of the same element with the same atomic population N_i. By following this approach, the assigned atomic densities quickly converge to a multipole expansion of the quantum mechanical electrostatic potential, resulting in chemically reasonable atomic populations [33].

Building on this charge partitioning the bond orders between all atomic couples are computed by estimating the overlap between their atomic densities; then, to estimate the reactivity of a given atom, all its bond orders are summed up to provide the so called Sum of Bond Orders (SBO) [34]. Therefore, the SBO, representing the total number of electrons that an atom shares in bonds, provides key insights into chemical reactivity trends. For example, a carbon atom tends to have a SBO of ∼4, since it has four valence electrons to share in covalent bonding. However, when we consider a carbon monoxide (CO) molecule, it exhibits a carbon SBO of only 2.58 and is more reactive than within CO_2, where its SBO is ∼4.

3. Results and discussion

3.1. Bond order analysis for Cu(111), C(111) and Pandey

The comparison between the SBO of surface atoms and those of atoms belonging to central layers, exhibiting bulk-like behavior, provides insights into surface reactivity. The SBO analysis of the clean Cu(111), C(111) and Pandey surfaces is reported in Table 1. As the slabs are symmetric, the SBO was calculated for half of the layers, ranging from the surface layer to the most central layer. We considered a 2×2 slab, each layer thus contains 4 atoms, which exhibit the same SBO in the unreconstructed diamond and copper slabs, but are not equivalent in the Pandey surface, resulting in different SBO values. In this case we provide the average SBO and its semidispersion. The SBO of carbon and copper atoms in their bulk geometry is 3.7 and 3.1 respectively, close to the ideal values as also reported in Ref. [34]. The results collected in Table 1, confirm that we are working with well converged slabs, since the SBOs of central layers are equal to those of the bulks. Moreover, the SBO of surface carbon atoms show that the C(111) surface is much more reactive than the Pandey one for which surface atoms have SBO∼4, indicating that all valence electrons are engaged in bonds. On the other hand, it is well known that surface atoms of unreconstructed diamond have an unpaired electron, which makes the surface highly reactive.

Also for Cu(111), the SBO of surface layers is reduced with respect to the bulk value, as expected.

3.2. Adatom adsorption on Cu(111), C(111) and Pandey

To incorporate chemical species at the interface, we started by identifying the most favorable adsorption sites. We considered a 25% surface coverage by including one adatom per (2×2) cell. The adatom adsorption energy is calculated as:

$$E_{ads} = E_{slab+a} - E_{slab} - E_a. \tag{3}$$

All the terms on the right side of the equation are total energies, namely, E_{slab+a} refers to the slab with the adsorbed atom, which we will also call decorated slab, whereas E_{slab} refers to the clean slab and E_a to the adatom. E_a can be obtained in two different ways: taking into account an isolated adatom or, to include the adatom-adatom interaction within a 25% coverage, by constructing the adatom array. In the first case, the adatom is placed in a large enough cubic box in order to prevent interactions with the replicas; in the latter case, the adatom is placed in the, otherwise empty, slab supercell.

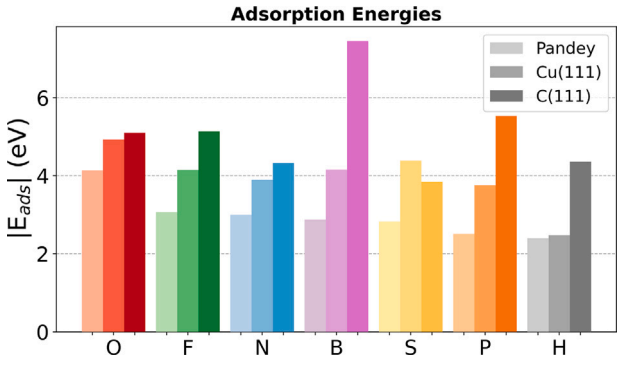

Fig. 2. Comparison between energy gain for adsorption of adatoms on the three considered surfaces. The histograms with the lighter area correspond to adsorption on Pandey-reconstructed surface, those with the medium shading represent adsorption on copper and the ones with the darker area indicate adsorption on C(111) surface.

To find the optimal adsorption site (i.e. the one displaying the lowest adsorption energy), the surfaces high symmetry points, shown in Fig. 1, are sampled. For all adsorbates species, the optimal adsorption site on Cu(111) turned out to be the hollow fcc, a high-coordination site. On C(111) the situation is more heterogeneous: B and P adsorb on the hollow hcp site, F, O and H on the top site, whereas N, S and Cu on the hollow fcc site. On the Pandey surface, during relaxation F, B and P move towards specific non high symmetry sites reported in Fig. 1, while, H adsorbs on the on top position and all the other adatoms on the bridge position between top atoms (bridge 1).

The energy gains resulting from the adsorption of the considered atomic species on Cu(111), C(111) and Pandey surfaces, calculated considering the adatom arrays, are collected in Fig. 2. With the only exception of S that adsorbs more favorably on copper, adsorption is always more favorable on the C(111) surface, while least adsorption energies are found on the Pandey surface due to its chemical inertness. A more detailed analysis of adatom adsorption on a case-by-case basis is provided in the Supplemental Material.

3.2.1. Work function analysis

The adsorption process induces the rearrangement of surface partial charges, causing a variation of the surface dipole, and thus the modification of the work function. Work function changes caused by adsorbates are important in various applications: they are used, for instance, to enhance the efficiency of cathode surfaces in fluorescent lamps [35,36], or to directly affect the electrode potential in electrochemistry applications [37,38]. Consequently, measuring adsorption-induced work function changes $\Delta\Phi$ is a standard practice in characterizing adsorbate systems [39].

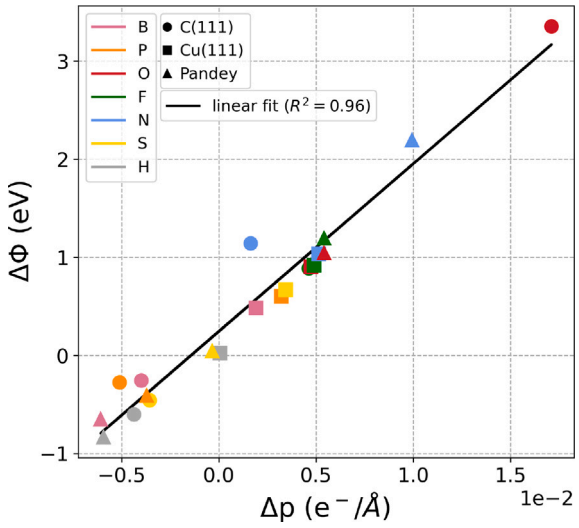

Fig. 3. Change in the work function versus dipole moment density variation induced upon adsorption for all the considered adsorbates, indicated with different colors, on Cu(111) (squares), C(111) (circles) and Pandey (triangles) surfaces.

In this work, following the approach described in Roman et al. [40] and Fatti et al. [18], the surface dipole is analyzed in terms of the charge density difference induced by adsorption:

$$\Delta\rho(\mathbf{r}) = \rho_{slab+a}(\mathbf{r}) - \rho_{slab}(\mathbf{r}) - \rho_a(\mathbf{r}) \tag{4}$$

where ρ_{slab+a} is the charge density of the adsorbate system, ρ_{slab} is the charge density of the clean surface and ρ_a is the charge density of the isolated adatom.

The dipole variation induced by adsorption is then defined as:

$$\Delta p(z) = \int_{bulk}^{vac} z\Delta\rho(z)\,dz \tag{5}$$

where the integration ranges from the center of the slab up to the middle of the vacuum and $\Delta\rho(z)$ is the x-y planar average of $\Delta\rho(\mathbf{r})$.

The work function Φ is defined as the difference between the vacuum level E_{vac} and the Fermi level E_F. Work function variations, given by the difference between the work functions of the surface-adsorbate systems and the clean surface: $\Delta\Phi = \Phi_{ads} - \Phi_0$, are analyzed. Our results are obtained considering dipole corrections, in order to cancel spurious electrostatic interactions in the vacuum region that, in some cases, strongly affect the value of E_{vac}. It is worth noting that dipole corrections do not affect strongly $\Delta\rho(z)$.

As predicted by Leung et al. [41] and shown in Fig. 3, a linear relation between $\Delta\Phi$ and Δp is found with a slope of 170.9 eV·Å/e$^-$, similar to the result reported for N, P, S, O adsorbed on Fe(110) [18] and to the predicted value of 180.95 [41].

The work function change of sign can be interpreted in terms of relative electronegativities between the adatom and the substrate. Indeed, for the simple case of atomic species adsorption such difference determines the orientation of the surface dipole therefore making it easier or more difficult for electrons to be extracted from the bulk. For the copper surface, $\Delta\Phi$ is always positive, in accordance with the fact that Cu is the less electronegative species. On the other hand, when diamond surfaces are involved, negative values of $\Delta\Phi$ are found for B, P, H and S adsorption which are the atomic species with lower electronegativity with respect to carbon.

3.3. Effect of reconstruction on c/cu adhesion

The optimal geometries of C(111)/Cu(111) and Pandey/Cu(111) interfaces are identified by sampling non-equivalent lateral positions between the two slabs. In both cases, the different configurations are obtained by shifting the copper slab so that its surface atoms are aligned with the high symmetry points of the diamond slab. The geometries with the lowest total energies are depicted in Fig. 4 (left). The optimal configuration for non-reconstructed diamond/copper interface has Cu atoms on top of diamond atoms, in agreement with Ref. [42]. The interfacial distance between Cu and diamond layers of 2.06 Å, compatible with Ref. [43], is shorter than 2.13 Å, the interlayer distance for bulk Cu along the (111) direction, suggesting that the interactions between Cu and C atoms could be stronger than those between Cu(111) bulk atoms. On the other side, the final geometry for the Pandey/copper interface shows surface Cu atoms on the bridges sites of C chains, with an interfacial distance of 2.19 Å, larger than the previous interface.

Table 2
Adhesion energies calculated with Eqs. (6) and (7) of clean interfaces. The last column reports the difference between the two to quantify the contribution of lattice distorsion.

Interface	E_{adh} (J/m^2)	$\widetilde{E}_{adh}$ (J/m^2)	Δ (J/m^2)
C(111)/Cu(111)	−2.67	−2.97	0.29
Pandey/Cu(111)	−0.43	−0.70	0.27

The adhesion energy per unit area is defined as follows:

$$E_{adh} = \frac{1}{A}(E_{12} - E_1 - E_2) \tag{6}$$

where A is the supercell area, E_{12} is the total energy of the relaxed heterogeneous interface, and E_1 and E_2 are the total energies of the relaxed isolated slabs.

Both the effect of surface–surface interactions and that of lattice deformations contribute to E_{12}. Indeed a poor E_{adh} could be the result of significant distortions in the slab lattices and/or of lack of interactions. Therefore, we separate the two effects by writing $E_{12} = \widetilde{E}_1 + \widetilde{E}_2 + \Delta E^{int}$, where $\widetilde{E}_i = E_i + \Delta E_i^{def}$ is the total energy of the i–th isolated slab in the distorted geometry in which it is stable within the interface. In this way it is possible to introduce a modified adhesion energy:

$$\widetilde{E}_{adh} = \frac{1}{A}(E_{12} - \widetilde{E}_1 - \widetilde{E}_2) = \frac{1}{A}\Delta E^{int} \tag{7}$$

where the effects of geometry deformations are left out.

The results for clean interfaces are shown in Table 2. The effect of lattice distorsions on adhesion is the same for both the Pandey and unreconstructed cases. This allows, in this specific case, to refer indifferently to E_{adh} or $\widetilde{E}_{adh}$ when analyzing the different amount of interactions happening in the interfacial region.

Adhesion energy of Pandey/Cu(111) interface is much smaller, in absolute value, than C(111)/Cu(111) one and this can be explained in terms of surface reactivity, which is strongly affected by Pandey reconstruction. Upon reconstruction, the atoms belonging to the first three atomic layers of the (111) surface of diamond significantly rearrange, in such a way that undercoordinated atoms are found as nearest neighbors in the first layer chains. The electrons on the chain atoms then partially dehybridize to 3 sp^2 and 1 p$_z$ orbitals, so that the p$_z$ dangling bonds can saturate each other through delocalized π orbitals. With respect to the unreconstructed surface, dangling bonds are thus eliminated, making the surface more inert. This leads to a reduced absolute value of the surface energy γ, which in turn corresponds to lower adhesion. Indeed, for clean interfaces, the behavior of adhesion can be inferred to a good extent from the knowledge of the surface energies of the single surfaces [44].

Our results confirm that adhesion reduction is possible, in general, by increasing the surface graphitization, which can be present in materials with higher sp^2/sp^3 ratio or after a rubbing action on the diamond surface. Indeed, it has been shown that the presence of graphitic material, such as aromatic molecules, is effective in reducing friction [45–49].

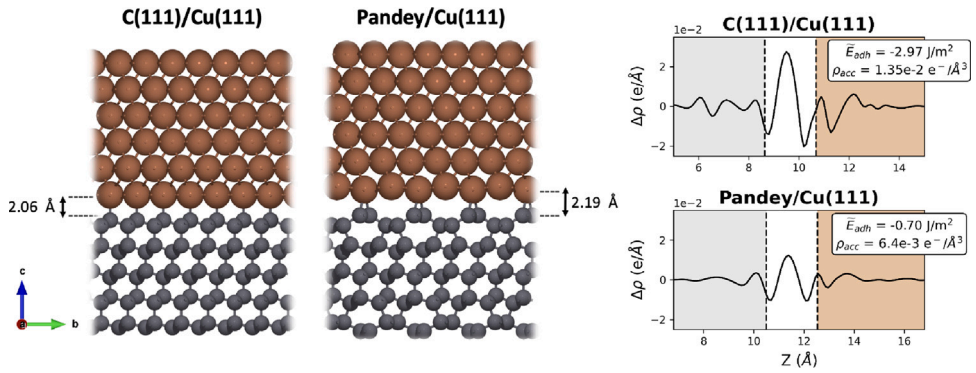

Fig. 4. On the left side, the optimal geometries of the clean C(111)/Cu(111) and Pandey/Cu(111) interfaces are shown. On the right side, planar averages of the charge density difference for the two systems are plotted using the same scale. The gray and orange areas represent diamond and copper regions, respectively. Adhesion energies and charge density accumulation values are also reported.

3.3.1. Charge density accumulation of clean interfaces

The tribological behavior of solid interfaces can often be correlated to their electronic properties [50]. In particular, it was shown that adhesion and frictional forces are strictly related to the electronic charge accumulation ρ_{acc} occurring at the interface and defined by the following procedure.

First the charge density difference $\Delta\rho$ is determined as:

$$\Delta\rho(\mathbf{r}) = \rho_{12}(\mathbf{r}) - \rho_1(\mathbf{r}) - \rho_2(\mathbf{r}) \tag{8}$$

where $\rho_{12}(\mathbf{r})$ is the charge density of the interface, while $\rho_1(\mathbf{r})$ and $\rho_2(\mathbf{r})$ are the charge densities of single surfaces.

Planar averages of the charge difference are shown as a line profile in the direction normal to the interface in Fig. 4 (right), allowing a first qualitative view of where the greatest charge redistribution upon interface formation is found: charge near the surfaces is depleted and accumulated in the interface region. Secondly, in order to quantify and be able to compare the magnitude of the accumulation of electronic charge density, the absolute value of the profile of $\Delta\rho(z)$ is integrated in the z direction over the length of the interfacial region, defined as the region between the highest atomic layer of the bottom slab (at $-z_0$) and the lowest atomic layer of the upper slab (at z_0), and normalized with respect to its width:

$$\rho_{acc} = \frac{1}{2z_0}\int_{-z_0}^{z_0} |\Delta\rho(z)|\, dz \tag{9}$$

The values of ρ_{acc} are reported in Fig. 4 (right), along with the corresponding adhesion energy of the interfaces. In accordance to what found in Ref. [50], a lower accumulation of electronic charge density corresponds to a lower interface adhesion, suggesting that ρ_{acc} can be a good descriptor to control not only adhesion but also friction. Indeed, in Ref. [50] it has been demonstrated that interfacial charge density and its variation during sliding are directly related to the Potential Energy Surface (PES) profiles, moreover PES corrugation, and ideal shear and cleavage strengths are related by simple linear and power laws to the adhesion itself [51].

3.4. Effect of chemical species intercalation on C/Cu adhesion

For each adatom, the decorated interfaces were built mating the slab/adatom system with lowest adsorption energy and the clean countersurface. The latter is then shifted to sample the different lateral positions, fully relaxing the interface, the most stable one being the one considered for calculating the adhesion energy.

In the case of a decorated interface, adhesion energies are calculated with Eqs. (6) and (7), where E_1 and E_2 are the total energies of the slab with the adsorbed adatom and of the clean countersurface, respectively.

3.4.1. C(111)/Cu(111)

In the C(111)/Cu(111) interface, according to the previously defined protocol and referring to the adsorption energies of Fig. 2, all adatoms are placed in their optimal adsorption site which is, for all cases, on the diamond slab with the exception of S, that adsorbs more favorably on Cu. We report in Section 8 of S.I. the case in which S:C(111)/Cu(111) is built starting with S adsorbed on diamond.

The relaxed optimal geometries of the considered decorated interfaces are shown in Fig. 5(a). In the case of B, P and H decorated interfaces, the register of the C/Cu surfaces corresponds to the favorable geometry in the clean interface: surface Cu atoms are on top of C atoms. In the O decorated interface, the register between the two surfaces seems dictated by the fact that the 4th Cu atom, which is not bonded to O, is adsorbed on the C slab in its optimal site (hollow fcc). Intercalation of N leads to a significant rearrangement of C surface atoms. In most cases, the Cu atoms within the surface undergo a rearrangement to accommodate the strong Cu-C bonds and comply with the additional coordination provided by the adatom to the Cu surface atoms in its proximity. Sulfur and fluorine act in a different way: they do not cause surface atoms distorsion and lead to an increase in the C–Cu distance of 1.66 and 1.96 Å, respectively. In particular, F is capable of moving the Cu surface away; an effect that can be explained by the electronic configuration of fluorine, which leads to fully saturated sp^3-type bonds between F and C atoms, making the surface inert. The structural consequences resulting from S intercalation can be attributed to its steric hindrance combined with its electronic configuration ($3s^2 3p^4$). Indeed, thanks to its possibility of having a valence equal to 4, S performs 3 bonds with the Cu nearest atoms and closes the single dangling bond of the carbon atom placed exactly on top of it (this hypothesis will be confirmed by the Bond Order calculation in Section 3.5.).

Values of adhesion energies and interface distances, calculated as the difference between the mean z values of C and Cu atoms in the surface layers, are reported in Table 3. Variations with respect to clean interface values are shown, together with E_{adh}-$\widetilde{E}_{adh}$ difference which quantifies the destabilization due to lattice distorsions. P and N are the ones causing a major structural deformation: without considering the distorsion effect we could have wrongly inferred that P reduces the surface-surface interactions more than H and N (looking solely at E_{adh} values).

In Fig. 6(a) the percentage variations of $|\widetilde{E}_{adh}|$ with respect to the clean interface are shown. Since the non-reconstructed diamond surface is extremely reactive and unstable all adatoms act as adhesion quencher, but fluorine and sulfur are the ones causing the most relevant drop, reducing adhesion of 96% and 74%, respectively. This result suggests that F could play an important role as adhesion-reducing element at interfaces, in accordance to what found in literature [52,53]. Similarly, the effective role of S as a lubricant additive has been proven also for Fe/Fe interfaces: when adsorbed on steel or iron surfaces, sulfur strongly reduce adhesion and ideal shear strength [54].

Table 3
Adhesion energies E_{adh} and $\widetilde{E}_{adh}$ calculated with Eqs. (6) and (7) of decorated C(111)/Cu(111) interfaces. Interfaces are ordered by their $\widetilde{E}_{adh}$ values. ΔE_{adh} and $\Delta\widetilde{E}_{adh}$ are the differences with respect to the clean counterpart. E_{adh}-$\widetilde{E}_{adh}$ quantifies the destabilization due to lattice distorsions. The interfacial distance is reported in the last column.

C(111)/Cu(111)	E_{adh} (J/m^2)	ΔE_{adh} (J/m^2)	$\widetilde{E}_{adh}$ (J/m^2)	$\Delta\widetilde{E}_{adh}$ (J/m^2)	E_{adh}-$\widetilde{E}_{adh}$ (J/m^2)	Distance (Å)
clean	−2.67	0	**−2.97**	0	0.29	2.06
O	−1.97	0.70	**−2.78**	0.18	0.81	2.40
B	−1.64	1.03	**−2.63**	0.33	0.99	2.35
P	−0.82	1.85	**−2.39**	0.58	1.57	3.02
N	−1.15	1.52	**−2.38**	0.59	1.23	2.52
H	−1.60	1.07	**−2.24**	0.73	0.64	2.44
S	−0.61	2.06	**−0.77**	2.20	0.16	3.72
F	−0.008	2.66	**−0.12**	2.84	0.11	4.02

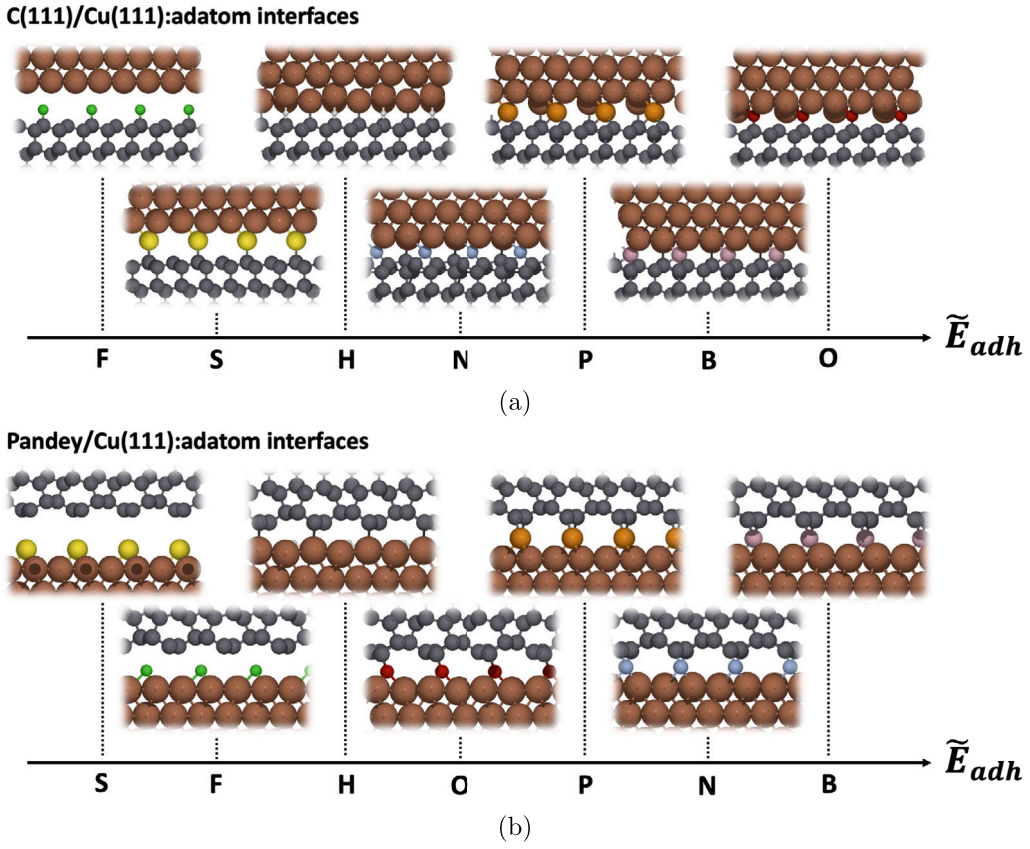

Fig. 5. Representation of the optimal geometries of **(a)** C(111)/Cu(111):adatom and **(b)** Pandey/Cu(111):adatom interfaces.

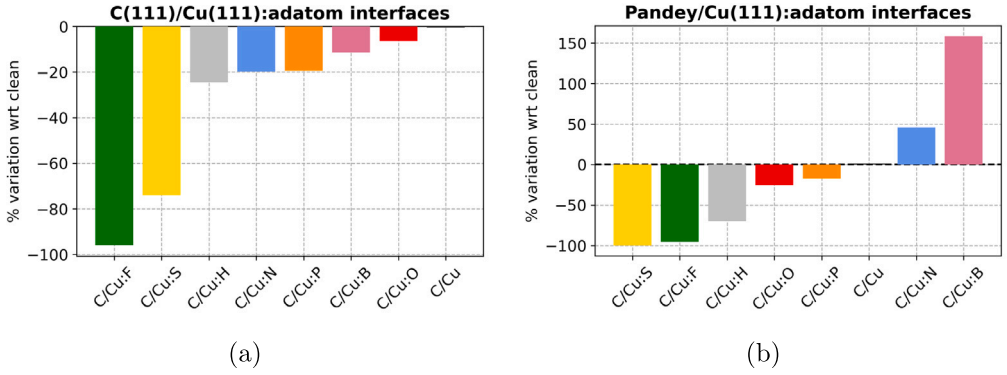

Fig. 6. Percentage variation of $|\widetilde{E}_{adh}|$ with respect to the clean value for **(a)** C(111)/Cu(111):adatom and **(b)** Pandey/Cu(111):adatom interfaces.

3.4.2. *Pandey/Cu(111)*

The most stable geometry of the Pandey/Cu(111):adatom interface is identified placing each adatom at its adsorption site on the copper slab and scanning the four inequivalent relative shifts of the diamond slab that align its high symmetry points to the adatom. The relaxed optimal geometries of the decorated interfaces are shown in Fig. 5(b).

Table 4
Adhesion energies E_{adh} and $\widetilde{E}_{adh}$ calculated with Eqs. (6) and (7) of decorated Pandey/Cu(111) interfaces. Interfaces are ordered by their $\widetilde{E}_{adh}$ values. ΔE_{adh} and $\Delta\widetilde{E}_{adh}$ are the differences with respect to the clean counterpart. E_{adh}-$\widetilde{E}_{adh}$ quantifies the destabilization due to lattice distortions. The interfacial distance is reported in the last column. The values of E_{adh} marked with (*) were set to 0 because slightly positive (0.03 J/m^2 for S, 0.008 J/m^2 and 0.005 J/m^2 for O and H, respectively). These slightly positive values can be attributed to numerical effects.

Pandey/Cu(111)	E_{adh} (J/m^2)	ΔE_{adh} (J/m^2)	$\widetilde{E}_{adh}$ (J/m^2)	$\Delta\widetilde{E}_{adh}$ (J/m^2)	E_{adh}-$\widetilde{E}_{adh}$ (J/m^2)	distance (Å)
B	−1.42	−0.99	**−1.81**	−1.11	0.39	3.0
N	−0.61	−0.18	**−1.02**	−0.33	0.41	3.01
clean	−0.43	0	**−0.70**	0	0.27	2.19
P	−0.19	0.24	**−0.58**	0.11	0.39	3.52
O	0*	0.44	**−0.52**	0.17	0.53	2.95
H	0*	0.43	**−0.21**	0.48	0.22	2.34
F	−0.006	0.42	**−0.03**	0.66	0.03	3.73
S	0*	0.46	**0.0004**	0.70	0.03	5.08

It is possible to see that F and especially S intercalations lead to a considerable increment in the distance between the slabs: 1.54 Å and 2.89 Å, respectively.

All the adatoms remain in their adsorption site (hollow fcc) on the Cu side. The relative position of the adatoms with respect to the Pandey-reconstructed surface are shown in Fig. 2 in the S.I.

In contrast with the C(111)/Cu(111):adatom interfaces, here strong rearrangements of the surface structures in order to form C–Cu bond are not present, since the Pandey-reconstructed surface is extremely inert.

As in the previous case, adhesion energies, variations with respect to clean interface values, effect of lattice distorsions and interfacial distances are reported in Table 4. In this case, oxygen is the one provoking the major lattice distorsion.

Percentage variations of $|\widetilde{E}_{adh}|$ with respect to the clean case are shown in 6(b): interestingly, for this interface, N and especially B act as adhesion enhancers, with an increase of the adhesion of 46% and 159%, respectively. The strong effect of B can be due to its flexibility in bond formation, attributed to the presence of a vacant p orbital in trivalent boron compounds [55]. This is indeed consistent with recent findings that B plays a significant role as grain-boundary strengthener [56] and is effective in improving strength, durability and wear resistance of Fe-based alloys [57–59]. Nitrogen, as well, is known for its ability to enhance the strength and wear resistance of stainless steel [60–62]. Its role as grain-boundary and strain hardener [63] makes it suitable for plenty industrial and biomedical applications [64].

S and F are the most effective in reducing adhesion: F decreases it by 96% (as in the case of C(111)/Cu(111)), while S completely eliminates it, maintaining a significant distance between the surfaces. From our results, it can be noticed that the roles of F and S as powerful adhesion reducers are universal and their effectiveness is independent of the degree of surface graphitization of diamond.

In the case of decorated interface, the increased complexity in terms of material types and nature of bonds makes the amount of charge density accumulation at the interface (ρ_{acc}) a less effective descriptor for the adhesion energy behavior (the complete analysis can be found in Section 7 of S.I.). Indeed, ρ_{acc} scales differently for different kinds of bonds and semiconducting species rearrange the charge much less uniformly than metallic ones [50]. A more detailed analysis of the bonding happening at the interface is therefore needed to gain insights on the mechanisms at play.

3.5. Bond order analysis

If BO_{ij} is the bond order between atom i and atom j, namely, the number of shared electrons in the ij bond, we define the bond order between diamond and copper slabs $BO_{\text{C-Cu}}$ by considering the total bond order of surface atoms, given by:

$$BO_{\text{C-Cu}} = \sum_{i=1}^{N}\sum_{j=1}^{M} BO_{ij} \tag{10}$$

where N and M are the total number of atoms in the surface layer of the two slabs. In our case, $N = M = 4$. Similarly, we can define the bond order between the intercalated adatom and one of the two slabs as the sum of bonds that adatom A forms with each surface atom: $BO_{A-X} = \sum_{j=1}^{M} BO_{Aj}$, where X stands for either C or Cu.

For clean interfaces, a higher C–Cu bond order corresponds to a stronger adhesion between the two slabs: $BO_{\text{C-Cu}}$~2.3 and ~1.7 for C(111)/Cu(111) and Pandey/Cu(111), respectively, in line with the electronic charge accumulation analysis.

In the case of decorated interface $BO_{\text{C-Cu}}$ is always smaller with respect to the clean interface values, because the presence of the adatoms inevitably keeps the surfaces more distant.

In Fig. 7 the surface-adatom and surface-surface bond orders are reported for the decorated Pandey interfaces (top panel) and C(111) interfaces (bottom panel). The interfaces are listed in ascending order with respect to $\Delta\widetilde{E}_{adh}$, i.e. the adhesion energy variation net of distorsion contributions. As expected, for each interface the adatom-surface BO is larger toward the slab providing the largest adsorption energy; however the adatom may also act as a chemical bridge providing a significant BO toward both surfaces at the same time. Moreover, the BO between Cu and C atoms may be significantly quenched or some amount of residual interaction might remain. As will be shown, the interplay between "adatom bridging" and residual interaction significantly affects adhesion.

In the case of decorated Pandey/Cu systems, the factor that most influences the adhesion variation is the ability of the adatom to form a bridge with the Pandey countersurface, while the residual interaction between the two surfaces is less decisive. Indeed, from Fig. 7(top panel) it is possible to see that both B and N enhance the adhesion because they form more bonds with the Pandey surface, allowing at the same time an interaction between the slabs which, although small, is nevertheless not negligible (~0.3). This is in accordance also with P behavior: it is the least effective in reducing adhesion because it forms a strong chemical bridge (BO_{A-C} ~1.7), but the C–Cu interaction is weaker with respect to N and B (~0.1). The decisive role of chemical bridging is evident in the case of O and H where it is low or absent: the strong C–Cu interaction in these cases still fails to compensate for the lack of a strong bond with the Pandey structure. Additionally, this analysis clearly reveals how F and S significantly reduce adhesion: both do not act as chemical bridges (BO_{A-C} ~0.1) and totally prevent surface interaction.

In the case of C(111)/Cu(111):adatom interfaces, all intercalated atomic species lead to a reduction in adhesion, given the high stability of the C/Cu interface. However, the previously discussed argument can be applied in this case as well, by analyzing the behavior of adatoms that are more or less effective in reducing the adhesion. In this case, our analysis reveals a more marked trade-off between chemical bridging and residual interaction. The results collected in the bottom panel of Fig. 7 show that both O and B, which are the least effective in adhesion reduction, act as bridges (BO_{A-Cu}~1.5) providing at the same time a high C–Cu bond order (~1.2). P and N, which are immediately next in the sequence, have a high interaction with the opposite copper slab (~1.8 and ~1.3, respectively), but allow less interaction between diamond and copper (~0.6 and ~0.4, respectively). H and S are the

	$\Delta\widetilde{E}_{adh}$(J/m^2)	A-C	A-Cu	C-Cu	Distance (Å)
B	-1.11	1.7	1.7	0.3	3.0
N	-0.33	1.9	1.2	0.3	3.01
P	0.11	1.7	2.1	0.1	3.52
O	0.17	1.1	1.3	0.4	2.95
H	0.48	0.09	1.1	1.3	2.34
F	0.66	0.1	1.0	0.1	3.73
S	0.7	0.1	2.4	0.0	5.08

(a)

	$\Delta\widetilde{E}_{adh}$(J/m^2)	A-C	A-Cu	C-Cu	Distance (Å)
O	0.18	1.1	1.5	1.2	2.4
B	0.33	1.6	1.5	1.2	2.35
P	0.58	1.8	1.8	0.6	3.02
N	0.59	1.6	1.3	0.4	2.52
H	0.73	0.7	0.4	1.7	2.44
S	2.2	1.0	3.1	0.09	3.72
F	2.84	1.0	0.2	0.08	4.02

(b)

Fig. 7. Bond order between adatom-C, adatom-Cu and C–Cu for **(a)** Pandey/Cu(111):adatom and **(b)** C(111)/Cu(111):adatom interfaces. The variation of the adhesion energy from the value of the clean interface, is reported. Positive values of $\Delta\widetilde{E}_{adh}$ means that the adatom acts as adhesion enhancer with respect to the clean configuration.

perfect examples of the mentioned trade-off. H provides the strongest interaction between C and Cu (~1.7) but forms a negligible chemical bond (comparable to that of F). In contrast, S, despite forming a slightly stronger bridge than H (note that S is the only case adsorbed on Cu), has a negligible residual C–Cu interaction, similar to that of F. This analysis also supports the earlier hypothesis that the 4-valence state of S allows it to form 3 bonds with Cu (BO_{A-Cu}~3.1) and a directional bond with the single dangling bond of the diamond (BO_{A-C}~1). Finally, F is the most effective element and is unique in not forming a bridge (BO_{A-Cu}~0.2) and preventing any interaction between the slabs (~0.08).

In conclusion, general observations can be drawn from the analysis of the bonding happening at the interface: (*i*) the residual interaction between the surfaces correlates with their distance; (*ii*) when a high degree of surface graphitization is present, diamond and copper surfaces do not interact per se, so the best way to increase adhesion is to find chemical species whose electronic configuration allows them to form multiple bonds with both surfaces involved (e.g., B and N). In this way, the atom acts as a chemical bridge, compensating for the lack of interaction between the surfaces. (*iii*) Thanks to its small size, H is the atom which keeps the slabs closer (2.34 Å for Pandey/Cu and 2.44 Å for C(111)/Cu), a characteristic which is directly connected to the highest values of C–Cu residual interaction. However, H is not able to form a chemical bridge and this is why it is quite effective in reducing adhesion in both scenarios. (*iv*) We can achieve ~100% of adhesion reduction if we select an atomic species that does not bond with the countersurface and prevents the interaction between the slabs (e.g., F and S). This is a general result, independent of the degree of surface graphitization.

4. Conclusions

In this work, non-reconstructed and Pandey-reconstructed C(111)/Cu(111) interfaces have been analyzed as representative models, in order to gain insights on the adhesion tuning of diamond and DLCs coatings on transition metal substrates through chemical modifications and surface reconstruction.

First, the adsorption analysis of the considered adatoms (B, P, F, O, H, N, S) on the three optimized surfaces (Cu(111), C(111) and Pandey) is performed: adsorption is always more favorable on the non-reconstructed diamond surface, with the only exception of sulfur that is the only atomic species adsorbing more favorably on copper. Adsorption on the Pandey-reconstructed surface is always less favorable with respect to the other two surfaces, due to its chemical inertness. Moreover, the analysis of the work function shows that a linear relation exists between the adsorption-induced work function change and the dipole variation with a slope of 170.9 eV·Å/e$^-$. The sign of the work function change can be easily interpreted in terms of relative electronegativities between the adatom and the substrate.

Then, adhesion energies of C(111)/Cu(111) and Pandey/Cu(111) interfaces are calculated, studying how they can be possibly tuned. In particular, we found that increasing surface graphitization causes a decreasing of the adhesion, associated with a less amount of electronic charge accumulation at the interface region. Adatom intercalation leads to adhesion quenching of diamond/DLC with surface sp^3 dangling bonds: fluorine and sulfur are the most effective, reducing adhesion of 96% and 74%. Moreover, also a fine tuning of the adhesion is possible by increasing surface graphitization and playing with atomic species intercalation. Indeed, both N and especially B increase the adhesion between Pandey and Cu(111) (increment of 46% and 159%, respectively), while S and F are, once again, the most powerful in reducing it (drop of 100% and 96%, respectively). In real conditions, surfaces usually reconstruct, are saturated or show faces with lower surface energies, thus we expect that the effect of B and N in increasing adhesion will be predominant with respect to their (not so effective) adhesion reduction effect on sp^3 like surface configurations.

The study of the bond order of atoms in the interface region allows to distinguish and quantify the different contributions to adhesion tuning, the primary factors at play being the adatom acting as a chemical bridge between the surfaces and the residual interaction left between the two. In particular, when a high degree of surface graphitization is present, diamond and copper surfaces do not interact per se, so the best way to increase adhesion is to find chemical species able to act as chemical bridges (e.g., B and N), compensating for the lack of interaction between the surfaces. On the contrary, adhesion reduction of ~100% can be achieved, regardless of the degree of surface graphitization, by

selecting an atomic species that does not bond with the countersurface and prevents the interaction between the slabs, i.e. F and S.

In this work, the use of a simplified model allowed an in-depth study of the fundamental mechanisms occurring at the interfacial region and our results already offer valuable insights on how to tune diamond and DLC coating adhesion in specific and controlled manners. Of course, often, devices, such as NEMS and MEMS, that would benefit from diamond coatings are exposed to air, making it interesting, for the future, to explore also more realistic models including metal oxides and different adatom coverages.

CRediT authorship contribution statement

Elisa Damiani: Writing – original draft, Investigation. **Margherita Marsili:** Writing – review & editing, Investigation. **M. Clelia Righi:** Writing – review & editing, Supervision, Funding acquisition, Conceptualization.

Declaration of competing interest

The authors declare that they have no known competing financial interests or personal relationships that could have appeared to influence the work reported in this paper.

Acknowledgments

These results are part of the "Advancing Solid Interface and Lubricants by First Principles Material Design (SLIDE)" project that has received funding from the European Research Council (ERC) under the European Union's Horizon 2020 research and innovation program (Grant agreement No. 865633).

E.D. acknowledges funding by the European Union - NextGenerationEU (National Sustainable Mobility Center CN00000023, Italian Ministry of University and Research Decree n. 1033 - 17/06/2022, Spoke 11 - Innovative Materials & Lightweighting). The opinions expressed are those of the authors only and should not be considered as representative of the European Union or the European Commission's official position. Neither the European Union nor the European Commission can be held responsible for them. All Authors acknowledge the CINECA award under the ISCRA initiative, for the availability of high performance computing resources and support.

Appendix A. Supplementary data

Supplementary material related to this article can be found online at https://doi.org/10.1016/j.carbon.2024.119555.

References

[1] R. Hauert, A review of modified DLC coatings for biological applications, Diam. Relat. Mater. 12 (3) (2003) 583–589, http://dx.doi.org/10.1016/S0925-9635(03)00081-5, 13th European Conference on Diamond, Diamond-Like Materials, Carbon Nanotubes, Nitrides and Silicon Carbide.

[2] G. Dearnaley, J. Arps, Biomedical applications of diamond-like carbon (DLC) coatings: A review, Surf. Coat. Technol. 200 (2005) 2518–2524, http://dx.doi.org/10.1016/j.surfcoat.2005.07.077.

[3] X. Yang, W. Zhang, X. Qin, M. Cui, Y. Guo, T. Wang, et al., Recent progress on bioinspired antibacterial surfaces for biomedical application, Biomimetics 7 (3) (2022) http://dx.doi.org/10.3390/biomimetics7030088.

[4] J. Robertson, Diamond-like amorphous carbon, Mater. Sci. Eng. R 37 (4) (2002) 129–281, http://dx.doi.org/10.1016/S0927-796X(02)00005-0.

[5] T.W. Scharf, S.V. Prasad, Solid lubricants: a review, J. Mater. Sci. 48 (2012) 511–531, URL https://api.semanticscholar.org/CorpusID:135902634.

[6] C. Love, R. Cook, T. Harvey, P. Dearnley, R. Wood, Diamond like carbon coatings for potential application in biological implants—a review, Tribol. Int. 63 (2013) 141–150, http://dx.doi.org/10.1016/j.triboint.2012.09.006.

[7] O. Auciello, J. Birrell, J.A. Carlisle, J.E. Gerbi, X. Xiao, B. Peng, et al., Materials science and fabrication processes for a new MEMS technology based on ultrananocrystalline diamond thin films, J. Phys.: Condens. Matter. 16 (16) (2004) http://dx.doi.org/10.1088/0953-8984/16/16/R02.

[8] Y.H. Lee, P.D. Richard, K.J. Bachmann, J.T. Glass, Bias-controlled chemical vapor deposition of diamond thin films, Appl. Phys. Lett. 56 (7) (1990) 620–622, http://dx.doi.org/10.1063/1.102716.

[9] A.G. Owens, S. Brühl, S. Simison, C. Forsich, D. Heim, Comparison of tribological properties of stainless steel with hard and soft DLC coatings, Proc. Mater. Sci. 9 (2015) 246–253, http://dx.doi.org/10.1016/j.mspro.2015.04.031.

[10] S.D.A. Lawes, M.E. Fitzpatrick, S.V. Hainsworth, Evaluation of the tribological properties of DLC for engine applications, J. Phys. D: Appl. Phys. 40 (18) (2007) 5427, http://dx.doi.org/10.1088/0022-3727/40/18/S03.

[11] R. Wang, C. Mercer, A. Evans, C. Cooper, H. Yoon, Delamination and spalling of diamond-like-carbon tribological surfaces, Diam. Relat. Mater. 11 (10) (2002) 1797–1803, http://dx.doi.org/10.1016/S0925-9635(02)00163-2.

[12] J.K. Luo, Y.Q. Fu, H.R. Le, J.A. Williams, S.M. Spearing, W.I. Milne, Diamond and diamond-like carbon MEMS, J. Micromech. Microeng. 17 (7) (2007) http://dx.doi.org/10.1088/0960-1317/17/7/S12.

[13] S. Peeters, A. Barlini, J. Jain, N.N. Gosvami, M. Righi, Adsorption and decomposition of ZDDP on lightweight metallic substrates: Ab initio and experimental insights, Appl. Surf. Sci. 600 (2022) http://dx.doi.org/10.1016/j.apsusc.2022.153947.

[14] E. Poli, M. Cutini, M. Nosir, O. Chehaimi, M. Righi, Effects of surface chemical modifications on the adhesion of metallic interfaces. An high-throughput first-principle analysis, Appl. Surf. Sci. 664 (2024) 160177, http://dx.doi.org/10.1016/j.apsusc.2024.160177.

[15] M. De La Pierre, M. Bruno, C. Manfredotti, F. Nestola, M. Prencipe, C. Manfredotti, The (100), (111) and (110) surfaces of diamond: an ab initio B3LYP study, Mol. Phys. 112 (7) (2014) 1030–1039, http://dx.doi.org/10.1080/00268976.2013.829250.

[16] A.A. Stekolnikov, J. Furthmüller, F. Bechstedt, Absolute surface energies of group-IV semiconductors: Dependence on orientation and reconstruction, Phys. Rev. B 65 (2002) 115318, http://dx.doi.org/10.1103/PhysRevB.65.115318.

[17] S. Yamamoto, A. Kawana, H. Ichimura, C. Masuda, Relationship between tribological properties and sp3/sp2 structure of nitrogenated diamond-like carbon deposited by plasma CVD, Surf. Coat. Technol. 210 (2012) 1–9, http://dx.doi.org/10.1016/j.surfcoat.2012.07.005.

[18] G. Fatti, P. Restuccia, C. Calandra, M.C. Righi, Phosphorus adsorption on Fe(110): An ab initio comparative study of iron passivation by different adsorbates, J. Phys. Chem. C 122 (49) (2018) 28105–28112, http://dx.doi.org/10.1021/acs.jpcc.8b08831.

[19] M. Spencer, I. Snook, I. Yarovsky, Coverage-dependent adsorption of atomic sulfur on fe(110): A DFT study, J. Phys. Chem. B 109 (19) (2005) 9604–9612, http://dx.doi.org/10.1021/jp044378l.

[20] P. Błoński, A. Kiejna, J. Hafner, Theoretical study of oxygen adsorption at the Fe(110) and (100) surfaces, Surf. Sci. 590 (1) (2005) 88–100, http://dx.doi.org/10.1016/j.susc.2005.06.011.

[21] G. Kresse, J. Hafner, Ab initio molecular dynamics for liquid metals, Phys. Rev. B 47 (1993) 558–561, http://dx.doi.org/10.1103/PhysRevB.47.558.

[22] G. Kresse, J. Furthmüller, Efficiency of ab-initio total energy calculations for metals and semiconductors using a plane-wave basis set, Comput. Mater. Sci. 6 (1) (1996) 15–50, http://dx.doi.org/10.1016/0927-0256(96)00008-0.

[23] G. Kresse, J. Furthmüller, Efficient iterative schemes for ab initio total-energy calculations using a plane-wave basis set, Phys. Rev. B 54 (1996) 11169–11186, http://dx.doi.org/10.1103/PhysRevB.54.11169.

[24] J.P. Perdew, K. Burke, M. Ernzerhof, Generalized gradient approximation made simple, Phys. Rev. Lett. 77 (1996) 3865–3868, http://dx.doi.org/10.1103/PhysRevLett.77.3865.

[25] A. Zur, T.C. McGill, Lattice match: An application to heteroepitaxy, J. Appl. Phys. 55 (2) (1984) 378–386, http://dx.doi.org/10.1063/1.333084.

[26] Y. Lu, G. Huang, L. Xi, Tribological and mechanical properties of the multi-layer DLC film on the soft copper substrate, Diam. Relat. Mater. 94 (2019) 21–27, http://dx.doi.org/10.1016/j.diamond.2019.02.019.

[27] S. Neuville, A. Matthews, A perspective on the optimisation of hard carbon and related coatings for engineering applications, Thin Solid Films 515 (17) (2007) 6619–6653, http://dx.doi.org/10.1016/j.tsf.2007.02.011.

[28] L. Qiang, B. Zhang, Y. Zhou, J. Zhang, Improving the internal stress and wear resistance of DLC film by low content ti doping, Solid State Sciences 20 (2013) 17–22, http://dx.doi.org/10.1016/j.solidstatesciences.2013.03.003.

[29] M. Ban, T. Hasegawa, S. Fujii, J. Fujioka, Stress and structural properties of diamond-like carbon films deposited by electron beam excited plasma CVD, Diam. Relat. Mater. 12 (1) (2003) 47–56, http://dx.doi.org/10.1016/S0925-9635(02)00265-0.

[30] E. Liu, L. Li, B. Blanpain, J.P. Celis, Residual stresses of diamond and diamondlike carbon films, J. Appl. Phys. 98 (7) (2005) 073515, http://dx.doi.org/10.1063/1.2071451.

[31] N.G. Limas, T.A. Manz, Introducing DDEC6 atomic population analysis: part 4. Efficient parallel computation of net atomic charges, atomic spin moments, bond orders, and more, RSC Adv. 8 (2018) 2678–2707, http://dx.doi.org/10.1039/C7RA11829E.

[32] L.P. Lee, N.G. Limas, D.J. Cole, M.C. Payne, C.-K. Skylaris, T.A. Manz, Expanding the scope of density derived electrostatic and chemical charge partitioning to thousands of atoms, J. Chem. Theory Comput. 10 (12) (2014) 5377–5390, http://dx.doi.org/10.1021/ct500766v.

[33] T.A. Manz, N.G. Limas, Introducing DDEC6 atomic population analysis: part 1. Charge partitioning theory and methodology, RSC Adv. 6 (2016) 47771–47801, http://dx.doi.org/10.1039/C6RA04656H.
[34] T.A. Manz, Introducing DDEC6 atomic population analysis: part 3. Comprehensive method to compute bond orders, RSC Adv. 7 (2017) 45552–45581, http://dx.doi.org/10.1039/C7RA07400J.
[35] J. Almanstötter, T. Fries, B. Eberhard, Electronic structure of fluorescent lamp cathode surfaces: BaO/W(001), J. Appl. Phys. 86 (1999) 325–328, http://dx.doi.org/10.1063/1.370732.
[36] A. Groß, The virtual chemistry lab for reactions at surfaces: Is it possible? will it be useful? Surf. Sci. 500 (1) (2002) 347–367, http://dx.doi.org/10.1016/S0039-6028(01)01526-6.
[37] S. Trasatti, The absolute electrode potential: an explanatory note (recommendations 1986), Pure Appl. Chem. 58 (7) (1986) 955–966, http://dx.doi.org/10.1351/pac198658070955.
[38] S. Schnur, A. Groß, Properties of metal–water interfaces studied from first principles, New J. Phys. 11 (12) (2009) http://dx.doi.org/10.1088/1367-2630/11/12/125003.
[39] P.K. Schmidt, K. Christmann, G. Kresse, J. Hafner, M. Lischka, A. Groß, Coexistence of atomic and molecular chemisorption states: H_2/Pd(210), Phys. Rev. Lett. 87 (2001) http://dx.doi.org/10.1103/PhysRevLett.87.096103.
[40] T. Roman, A. Groß, Periodic density-functional calculations on work-function change induced by adsorption of halogens on Cu(111), Phys. Rev. Lett. 110 (2013) http://dx.doi.org/10.1103/PhysRevLett.110.156804.
[41] T.C. Leung, C.L. Kao, W.S. Su, Y.J. Feng, C.T. Chan, Relationship between surface dipole, work function and charge transfer: Some exceptions to an established rule, Phys. Rev. B 68 (2003) http://dx.doi.org/10.1103/PhysRevB.68.195408.
[42] X.-G. Wang, J.R. Smith, Copper/diamond adhesion and hydrogen termination, Phys. Rev. Lett. 87 (18) (2001) http://dx.doi.org/10.1103/PhysRevLett.87.18610.
[43] Z. Liu, S. Zheng, Z. Lu, J. Pu, G. Zhang, Adhesive transfer at copper/diamond interface and adhesion reduction mechanism with fluorine passivation: A first-principles study, Carbon 127 (2018) 548–556, http://dx.doi.org/10.1016/j.carbon.2017.11.027.
[44] P. Restuccia, G. Losi, O. Chehaimi, M. Marsili, M.C. Righi, High-throughput first-principles prediction of interfacial adhesion energies in metal-on-metal contacts, ACS Appl. Mater. Interfaces 15 (15) (2023) 19624–19633, http://dx.doi.org/10.1021/acsami.3c00662.
[45] Y. Long, A. Pacini, M. Ferrario, N.V. Tran, S. Peeters, B. Thiebaut, et al., Superlubricity from mechanochemically activated aromatic molecules of natural origin: A new concept for green lubrication, Carbon 228 (2024) 119365, http://dx.doi.org/10.1016/j.carbon.2024.119365.
[46] S. Peeters, G. Losi, S. Loehlé, M. Righi, Aromatic molecules as sustainable lubricants explored by ab initio simulations, Carbon 203 (2023) 717–726, http://dx.doi.org/10.1016/j.carbon.2022.11.078.
[47] T. Kuwahara, P.A. Romero, S. Makowski, V. Weihnacht, G. Moras, M. Moseler, Mechano-chemical decomposition of organic friction modifiers with multiple reactive centres induces superlubricity of ta-C, Nature Commun. 10 (151) (2019) http://dx.doi.org/10.1038/s41467-018-08042-8.
[48] Y. Long, T. Kuwahara, M. De Barros Bouchet, A. Ristić, N. Dörr, T. Lubrecht, et al., In situ synthesis of graphene nitride nanolayers on glycerol-lubricated si3n4 for superlubricity applications, ACS Appl. Nano Mater. 4 (3) (2021) 2721–2732, http://dx.doi.org/10.1021/acsanm.0c03362.
[49] J. Li, X. Ge, J. Luo, Random occurrence of macroscale superlubricity of graphite enabled by tribo-transfer of multilayer graphene nanoflakes, Carbon 138 (2018) 154–160, http://dx.doi.org/10.1016/j.carbon.2018.06.001.
[50] M. Wolloch, G. Levita, P. Restuccia, M.C. Righi, Interfacial charge density and its connection to adhesion and frictional forces, Phys. Rev. Lett. 121 (2) (2018) http://dx.doi.org/10.1103/PhysRevLett.121.026804.
[51] M. Wolloch, G. Losi, M. Ferrario, M.C. Righi, High-throughput screening of the static friction and ideal cleavage strength of solid interface, Sci. Rep. 9 (2019) 17062, http://dx.doi.org/10.1038/s41598-019-49907-2.
[52] A.E. Somers, S.M. Biddulph, P.C. Howlett, J. Sun, D.R. MacFarlane, M. Forsyth, A comparison of phosphorus and fluorine containing IL lubricants for steel on aluminium, Phys. Chem. Chem. Phys. 14 (2012) 8224–8231, http://dx.doi.org/10.1039/C2CP40736A.
[53] S. Veldhuis, G. Dosbaeva, G. Benga, Application of ultra-thin fluorine-content lubricating films to reduce tool/workpiece adhesive interaction during thread-cutting operations, Int. J. Mach. Tools Manuf. 47 (3) (2007) 521–528, http://dx.doi.org/10.1016/j.ijmachtools.2006.06.003.
[54] M.C. Righi, S. Loehlé, M.I. De Barros Bouchet, S. Mambingo-Doumbe, J.M. Martin, A comparative study on the functionality of S- and P-based lubricant additives by combined first principles and experimental analysis, RSC Adv. 6 (2016) 47753–47760, http://dx.doi.org/10.1039/C6RA07545B.
[55] A. Bhunia, Boron has more surprises, Chem 6 (2) (2020) 320–321, http://dx.doi.org/10.1016/j.chempr.2020.01.017.
[56] A. Sharma, S. Dixit, N. Baler, P. Agrawal, S.K. Makineni, K. Chattopadhyay, Impact of boron as an alloying addition on the microstructure, thermo-physical properties and creep resistance of a tungsten-free co-base superalloy, Mater. Sci. Eng. A 855 (2022) http://dx.doi.org/10.1016/j.msea.2022.143899.
[57] L.Y.e.a. Liu Zl., High boron iron-based alloy and its modification, J. Iron Steel Res. Int. 16 (2009) 37–42, http://dx.doi.org/10.1016/S1006-706X(09)60041-8.
[58] M. Izaki, N. Miyamoto, A. Nakae, T. Hasegawa, S. Watase, M. Chigane, et al., Martensitic iron-carbon-boron alloy electrodeposit with improved mechanical properties, J. Electrochem. Soc. 149 (2002) http://dx.doi.org/10.1149/1.1484376.
[59] S. Ma, J. Zhang, Wear resistant high boron cast alloy - a review, 2016.
[60] H. Dimigen, K. Kobs, R. Leutenecker, H. Ryssel, P. Eichinger, Wear resistance of nitrogen-implanted steels, Mater. Sci. Eng. 69 (1) (1985) 181–190, http://dx.doi.org/10.1016/0025-5416(85)90390-8.
[61] T. Mattar, K.M. Ibrahim, A. Fathy, H. El Faramawy, Improving the wear resistance of M41 steel by nitrogen alloying and ESR, Mater. Charact. 58 (5) (2007) 407–415, http://dx.doi.org/10.1016/j.matchar.2006.06.007.
[62] H. Halfa, Microstructure–wear resistance relationship of nitrogen-containing high-speed tool steel, AISIM41: Non-equilibrium solidification, Metallogr. Microstruct. Anal. 11 (2022) 495–512, http://dx.doi.org/10.1007/s13632-022-00851-0.
[63] Y.X. Qiao, S.-L. Sheng, L. Zhang, J. Chen, L.-L. Yang, H.-L. Zhou, et al., Friction and wear behaviors of a high nitrogen austenitic stainless steel Fe-19Cr-15Mn-0.66N, J. Mining Metallur. Sect. B Metallur. 57 (2021) 25, http://dx.doi.org/10.2298/JMMB201026025Q.
[64] J. Corona-Gomez, S. Shiri, M. Mohammadtaheri, Q. Yang, Adhesion enhancement of DLC on CoCrMo alloy by diamond and nitrogen incorporation for wear resistant applications, Surf. Coat. Technol. 332 (2017) 120–127, http://dx.doi.org/10.1016/j.surfcoat.2017.10.050.